Metallothionein-Like Multinuclear Clusters of Mercury(II) and Sulfur in Peat

Kathryn L. Nagy,*,[†] Alain Manceau,[‡] Jarrod D. Gasper,[§,⊥] Joseph N. Ryan,[∥] and George R. Aiken[§]

[†]Department of Earth and Environmental Sciences, MC-186, 845 West Taylor Street, University of Illinois at Chicago, Chicago, Illinois 60607, United States

[‡]ISTerre-Maison des Géosciences, CNRS and Université J. Fourier, BP 53, 38041 Grenoble Cedex 9, France

[§]United States Geological Survey, Water Resources Discipline, 3215 Marine Street, Boulder, Colorado 80303, United States

[∥]Department of Civil, Environmental, and Architectural Engineering, University of Colorado Boulder, 428 UCB, Boulder, Colorado 80309-0428, United States

S *Supporting Information*

ABSTRACT: Strong mercury(II)—sulfur (Hg-SR) bonds in natural organic matter, which influence mercury bioavailability, are difficult to characterize. We report evidence for two new Hg-SR structures using X-ray absorption spectroscopy in peats from the Florida Everglades with added Hg. The first, observed at a mole ratio of organic reduced S to Hg (S_{red}/Hg) between 220 and 1140, is a Hg_4S_x type of cluster with each Hg atom bonded to two S atoms at 2.34 Å and one S at 2.53 Å, and all Hg atoms 4.12 Å apart. This model structure matches those of metal—thiolate clusters in metallothioneins, but not those of HgS minerals. The second, with one S atom at 2.34 Å and about six C atoms at 2.97 to 3.28 Å, occurred at S_{red}/Hg between 0.80 and 4.3 and suggests Hg binding to a thiolated aromatic unit. The multinuclear Hg cluster indicates a strong binding environment to cysteinyl sulfur that might impede methylation. Along with a linear $Hg(SR)_2$ unit with Hg—S bond lengths of 2.34 Å at S_{red}/Hg of about 10 to 20, the new structures support a continuum in Hg-SR binding strength in natural organic matter.
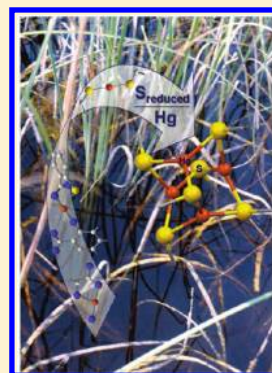
INTRODUCTION

Reduced sulfur (S_{red}) ligands are the main pool of strong binding sites for mercury(II) (Hg) in natural organic matter (OM) that may influence methylation rates, distribution and transport, and ecotoxicity of mercury. The S_{red} derives from biomolecules produced by organisms, free sulfide species formed during microbial sulfate reduction, and recycled products of OM degradation and diagenesis. Total amounts of S_{red} in OM range typically from about 0.1—2 wt %, sufficient to bind even unusually high concentrations of Hg.

Small organic and inorganic Hg—S_{red} species can enable methylation,[1,2] but effects of Hg bound to larger OM molecules on microbial methylation and direct toxicity to fish and filter-feeders are ambiguous or unknown.[3-5] Unlike small biomolecules, which are labile and can rapidly exchange thiol-bonded Hg,[6] macromolecular OM may have binding environments that are influential in decreasing bioavailability of Hg. Because peat and soil OM contain more macromolecular plant-derived compounds, as well as more reduced and total S, compared to dissolved OM (DOM), they may sequester Hg from the aqueous phase.

The binding strength of Hg to OM, expressed as conditional $HgLR^+$ and HgL_2R formation constants, spans from about 10^{10} to 10^{38},[7-14] corresponding to mole ratios of S_{red} to bound Hg (S_{red}/Hg) from less than 1 to about 77000 in the solid phase at equilibrium with dissolved mercury. In the form $Hg(LR)_2$ the largest constants are $\geq 10^{43}$, matching values for thiol-binding in low molecular weight organic molecules.[15] The strongest binding sites containing S_{red} are fewer in number than the markedly weaker sites containing O and/or N.[8]

Binding constants must be linked to molecular structures to quantify reactions between OM and Hg species. Such structures have been characterized in peat, soil OM, and humic acid with added metal using extended X-ray absorption fine-structure (EXAFS) spectroscopy. At mole ratios of S_{red}/Hg = 0.3 to 1.2 a structure with one S and one O or N bond (i.e., R(O/N)HgSR) was observed[16,17] whereas at S_{red}/Hg = 1.6 to 4, 60 to 90% of added Hg bonded to 1.3 to 1.7 S atoms, suggesting up to 70% $Hg(SR)_2$ in a linear configuration.[17] At S_{red}/Hg = 20 to 100 a $Hg(SR)_{2-3}$ complex with two S ligands at 2.34 Å and a tentative third near 3 Å in a T-shape geometry was reported.[18,19] Possible three-coordinate binding is supported by the average release of 2.7 protons for each adsorbed Hg atom in peat humic acid at S_{red}/Hg = 120.[13]

Peat typically contains about 0.1 ppm Hg (0.1 mg Hg/kg OM, equivalent to about 10^6 mol S_{red}/mol Hg). This amount of

mercury is about 1% of the adsorbed amount (10 ppm Hg) at which the strongest binding constants in OM have been measured,[8,9,12] and about 0.1% of the lowest value at which EXAFS spectra are measurable today. Because only about 0.02% of S_{red} is needed to bind 0.1 ppm Hg, molecular structures identified by EXAFS at around 100 ppm Hg, or about 20% of the S_{red}, may reasonably approximate the strongest sites. Our goal was to distinguish binding environments that involved S_{red} by obtaining and interpreting EXAFS spectra of Hg-containing peats, including spectra obtained at liquid He temperature.

The peats were collected from two locations (F1 and 2BS) in the Everglades that had different inorganic sulfide (HS$^-$) concentrations and Hg methylation rates.[20] They were shown to have dominantly strong to weak binding at adsorbed Hg concentrations over the range of 1−400000 ppm.[9] We observed two new molecular binding environments out of a total of four between 59 and 99100 ppm added Hg (S_{red}/Hg mole ratio from 1140 to 0.50) that expand our understanding of how the continuum of sulfur binding sites in OM may form and influence bioavailability of mercury.

■ EXPERIMENTAL SECTION

We adsorbed mercury to the peats using the experimental procedure described previously[9] except that the concentration of peat was 10 times higher (0.1 g peat in 0.25 L of solution) to obtain enough material for EXAFS spectroscopic analysis. Experiments were conducted at initial solution concentrations of mercury from 3×10^{-7} to 2×10^{-4} mol/L. Mercury was analyzed using cold vapor atomic fluorescence spectroscopy (PS Analytical Ltd., Kent, UK).

EXAFS spectra at the Hg-L$_3$ edge were recorded at room temperature (RT) and nine months later at liquid helium temperature (He-T; 8−16 K) at beamline BM30B (FAME) of the European Synchrotron Radiation Facility (ESRF) and analyzed by standard techniques. X-ray absorption near-edge structure (XANES) spectra at the S-K edge were recorded on unreacted peat at RT at beamline 10.3.2, Advanced Light Source (ALS). Fractional abundances of reduced and oxidized sulfur species were obtained by linear combination fitting of reference spectra. Binding structures for Hg were identified by comparing spectral features of samples to those of reference compounds, fitting sample spectra with linear combinations of spectra, and modeling Fourier-transformed k^3-weighted spectra using amplitude and phase shift functions calculated from first principles.

Details of the experiments and analyses are in the Supporting Information (SI).

■ RESULTS AND DISCUSSION

In contrast to the generally linear trend in the adsorption isotherms, which may be explained by at most two binding sites, the EXAFS spectral analysis revealed four structural binding environments, three of which involved sulfur ligands. Two of the binding environments identified are reported for the first time. One is a multinuclear Hg-SR coordination structure observed at low amounts of adsorbed Hg and the other is indicative of Hg bonded to thiolated aromatic subunits observed at high amounts of adsorbed Hg. We first present results for the adsorption isotherms and XANES spectra of the sulfur speciation in the peats, followed by results for the individual binding environments derived from the EXAFS spectra.
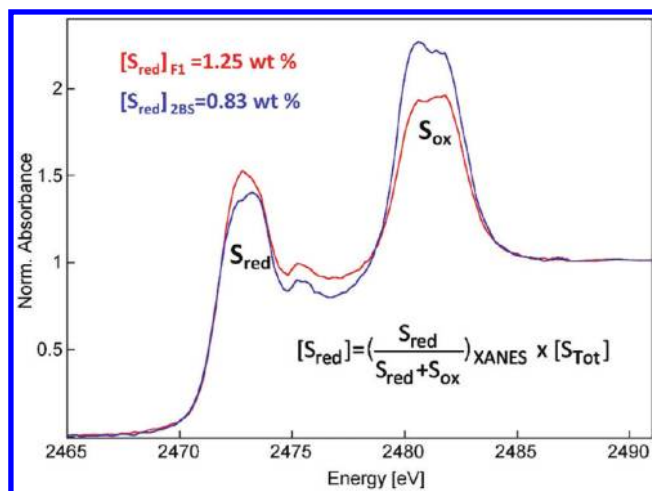

Figure 1. S-XANES spectra for F1 and 2BS peats. The peats were fit with approximately the same amounts of cystine (29−31%), sulfoxide (9−11%), and sulfate (6−7%), but F1 had more cysteine (41 vs 34%) and 2BS more sulfonate (23 vs 16%). The first difference is seen in the ratio of the peak amplitudes of reduced (S_{red}) to oxidized sulfur (S_{ox}), which is higher for F1 than 2BS, and the second in the asymmetrical shape of the oxidized sulfur peak for 2BS which crests at the energy of the sulfonate component (2480.5 eV).

S-XANES Spectra and Adsorption Isotherms. Initial values of the mole ratio S_{red}/Hg in the peats were 3×10^5 for 2BS and 8×10^5 for F1, where S_{red} was determined by XANES spectroscopy (Figure 1 and SI). The peats adsorbed 1 to 99100 ppm Hg (S_{red}/Hg = 78300 to 0.50, respectively) as aqueous Hg concentration increased, similarly to earlier observations[9] (SI). At low aqueous concentrations of Hg the F1 peat, which had more total and reduced S (1.79 wt % S_{Total}; 1.25 wt % S_{red}), adsorbed slightly more Hg than the 2BS peat (1.27 wt % S_{Total}; 0.83 wt % S_{red}). One inflection point between 10^{-8} and 10^{-7} mol Hg/L indicates the data might be fit with two Langmuir isotherms representing two binding sites.

EXAFS Spectra at Room Temperature. The k^3-weighted spectra of peats with 59−99100 ppm Hg (S_{red}/Hg = 1140 to 0.50) obtained at RT have features that differentiate three binding environments (Figure 2a). Two are evident by isosbestic points for samples having 4170 to 99100 ppm Hg, resulting from a rightward shift in oscillation frequency and a decrease in amplitude with increasing Hg concentration (Figure 2b). These features show that, with decreasing S_{red}/Hg mole ratio, Hg binding transitions from dominant longer bonds (short wave frequency) with S atoms to shorter bonds (long wave frequency) with atoms of smaller ionic radii (O, N).[17,18]

At any amount of Hg, the F1 spectrum is shifted slightly left of the 2BS spectrum to the point that F1-99 (99100 ppm) is more like 2BS-19 (19000 ppm) than 2BS-99 (99100 ppm). The systematic shift is related to the 50% more S_{red} in the F1 peat and confirms the significance of Hg−S bonds in the EXAFS signal even at high amounts of adsorbed Hg (i.e., low values of S_{red}/Hg).[16,17]

A third binding environment is indicated at lower Hg concentrations by slight leftward shifts of the oscillations, which imply even longer bonds (Figure 2c). This observation motivated measurements at He-T of six samples representing the variation in RT spectra and the spread of S_{red}/Hg values. Freezing slows the thermal motion of atoms, and for an
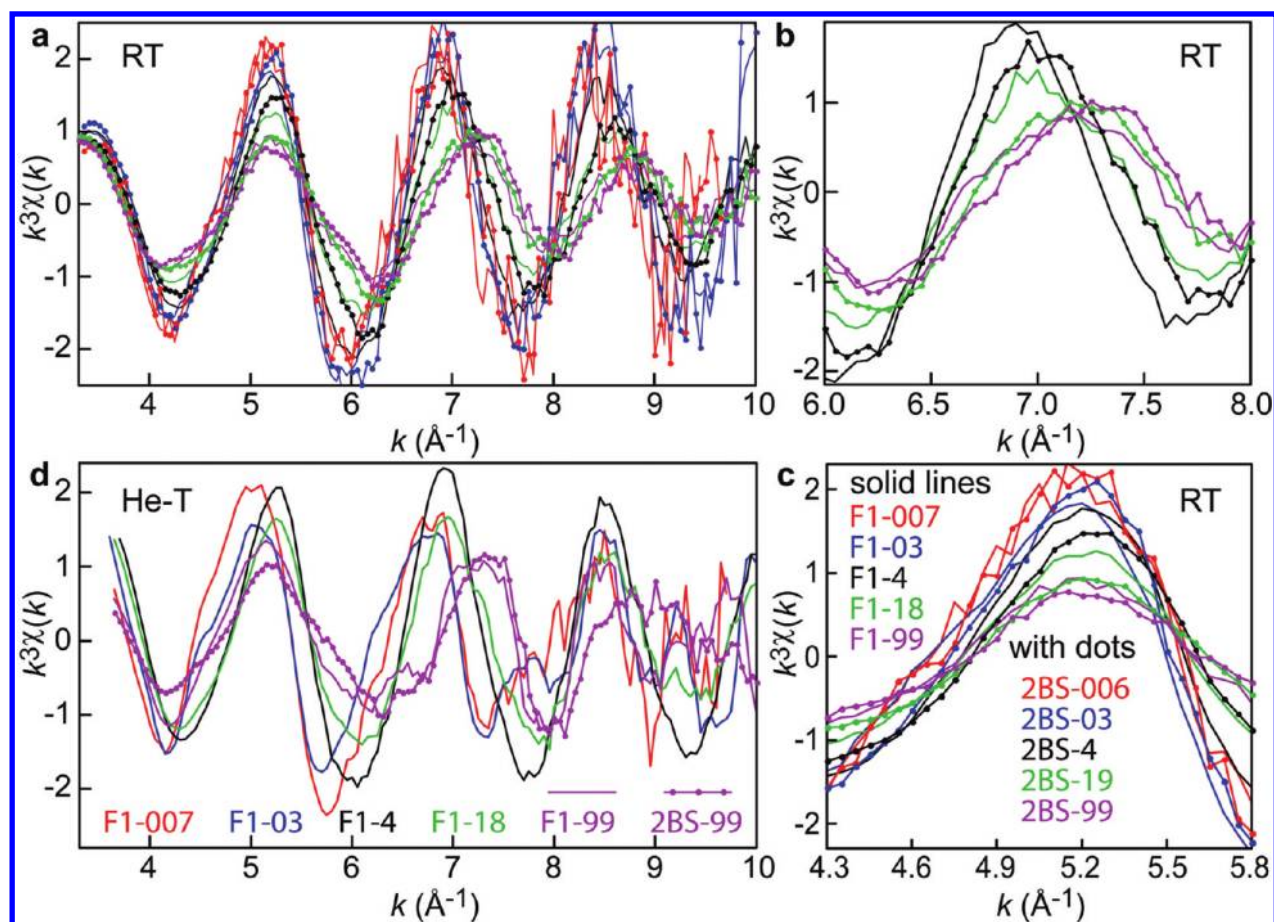
Figure 2. EXAFS spectra for F1 and 2BS peat samples. Sample code suffixes represent adsorbed Hg in ppm (mg Hg/kg peat): −006 and −007 (59 and 69 ppm); −03 (∼350 ppm); −4 (∼4100 ppm); −18 and −19 (18400 and 19000 ppm); −99 (99100 ppm) (SI). (a) Room temperature (RT) spectra cut at $k = 10\ \text{Å}^{-1}$ for clarity except for −006 and −007 spectra which were stopped at $k = 9.8\ \text{Å}^{-1}$ because of interfering absorbance at the Se K-edge. (b) RT spectra at $k = 6$ to $8\ \text{Å}^{-1}$ showing rightward shift to lower frequency at higher Hg concentration, signifying shorter Hg-ligand distances. Spectra at 59 to 350 ppm are omitted for clarity. (c) RT spectra at $k = 4.2$ to $5.6\ \text{Å}^{-1}$ showing leftward shift to higher frequency at lower Hg concentration, signifying longer Hg-ligand distances. (d) Spectra at liquid helium temperature (He-T) cut to $k = 10\ \text{Å}^{-1}$.

individual bond increases the amplitude of the EXAFS signal. Thus, we expected an improved signal-to-noise ratio and better resolution of interatomic distances at liquid He temperature.

EXAFS Spectra at Liquid He Temperature. At He-T, longer Hg—S bonds were more evident by the farther leftward shift of spectra at low Hg concentrations and sinistral asymmetry of the first two oscillations (Figures 2d and 3a). Other bonds, also more apparent at He-T, caused extra small oscillations at about $k = 7.8$ and $9.2\ \text{Å}^{-1}$ in F1-007 (69 ppm Hg; $S_{red}/Hg = 1140$) and F1-03 (353 ppm Hg; $S_{red}/Hg = 220$) (Figure 2d) and also at 10.6 and $12\ \text{Å}^{-1}$ in F1-03 (SI). Detailed analyses of the spectra and modeled coordination structures from low to high adsorbed Hg concentrations (i.e., high to low mole ratios of S_{red}/Hg) are presented below.

Multinuclear Hg—S Binding at Low Hg Concentration. The spectra of F1-03 and F1-007 changed the most between RT and He-T, implicating dominant soft metal-soft ligand Hg—S bonds. Fourier transforms of the F1-03 spectra show that (1) the peak at $R + \delta \approx 2\ \text{Å}$ (distance uncorrected for phase shift) with a small shoulder on the right at RT split into two peaks at about 1.8 and 2.3 Å and (2) the peak at about 4 Å increased in amplitude at He-T (Figure 3a). These changes are understood by comparison

to the changes in cinnabar (α-HgS) spectra between RT and He-T (Figure 3b).

At RT the spectrum of α-HgS is dominated by the signal from Hg—S bonds of length 2.38 Å ($R + \delta \approx 2\ \text{Å}$); the signal from Hg—Hg pairs at $R + \delta \approx 4\ \text{Å}$ is weak. At He-T the signal amplitude is higher and the local structure of α-HgS fully agrees with crystallographic data. Longer Hg—S bonds at 3.07 and 3.26 Å are detected, modeling shows two distinct Hg—Hg pairs at 3.79 Å and 4.11 Å, and longer Hg—Hg pairs at 5.67 and 6.82 Å appear (SI). Similar spectral features are seen in cinnabar spectra obtained at 77 K[21] (SI).

Changes for the F1 peats with temperature, although similar, are distinct from those for cinnabar. Differences include the out-of-phase patterns between $k \approx 10.2$ and $12.8\ \text{Å}^{-1}$ and the peak shapes at $R + \delta \approx 4\ \text{Å}$ at He-T. Using the cinnabar spectrum at He-T to guide bond assignments, two Hg—S bonds of length 2.34 Å and one of length 2.53 Å were derived from the F1-03 peat spectrum at He-T along with one Hg—C or Hg—S bond at 3.25 Å, and three Hg—Hg pairs at 4.12 Å (Figure 4a, SI). The counterintuitive weakening of spectral amplitude at low k values in F1-03 at He-T compared to RT is a result of the relative difference in enhancement of amplitude of the two Hg—S bonds at low temperature (SI).
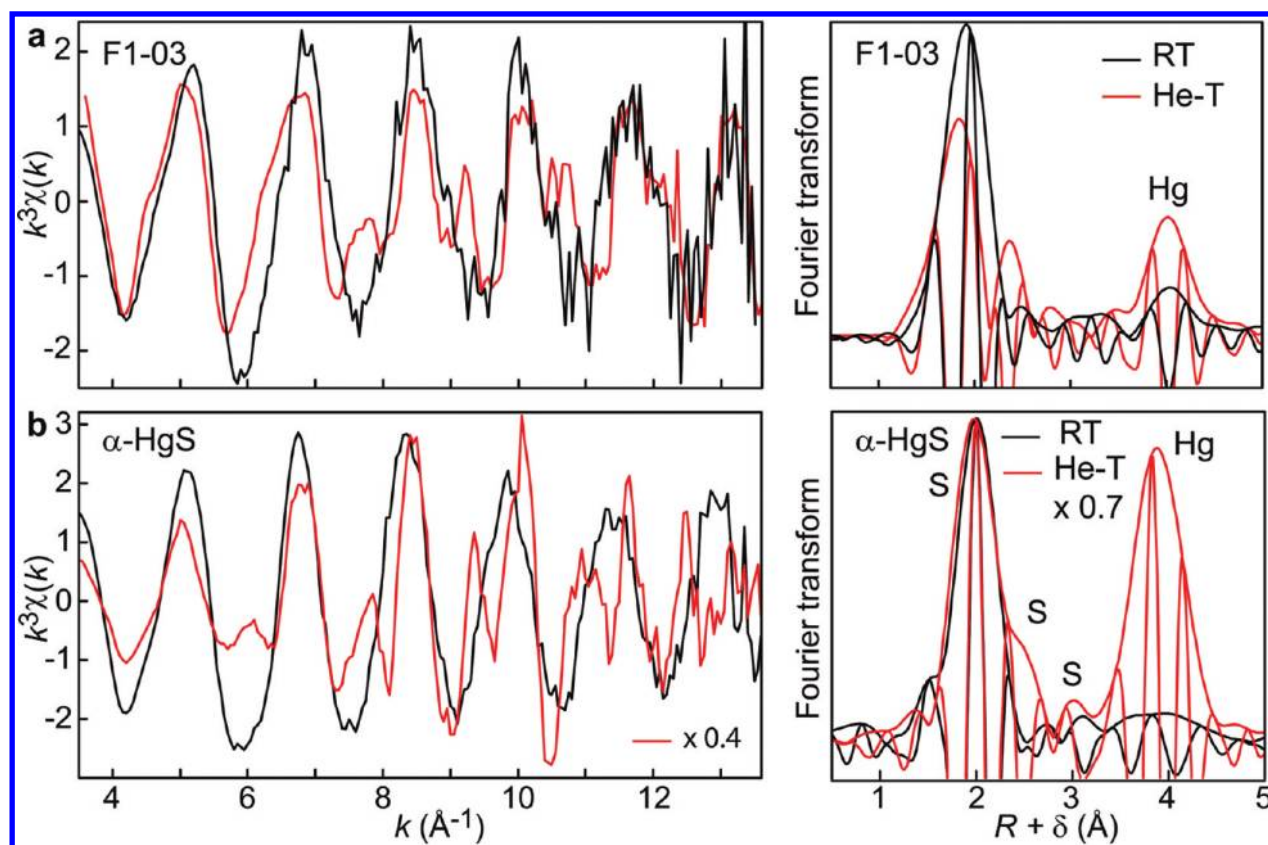
7300

dx.doi.org/10.1021/es201025v |Environ. Sci. Technol. 2011, 45, 7298–7306

Figure 3. EXAFS spectra (left) and Fourier transforms (right) for F1−03 peat (353 ppm Hg) and cinnabar (α-HgS). Imaginary parts of the Fourier transforms show that the differences in the EXAFS frequencies observed in k-space at RT and He-T come from the magnification at low temperature of distant Hg—S and Hg—Hg pairs. (a) F1-03 at RT and He-T. (b) α-HgS at RT and He-T. Amplitudes for the spectra and Fourier transforms of α-HgS were reduced by multiplicative factors to aid comparison of peak shapes and positions.

Comparison of the Hg-SR structure in the peat and metacinnabar (β-HgS) at He-T is also warranted, but is not straightforward. Although the spectra for metacinnabar and cinnabar (α-HgS) are distinct at RT, the spectrum of β-HgS is similar to that of cinnabar (α-HgS) at He-T, indicating that the structure of the metastable mercuric sulfide (β-HgS) approaches that of cinnabar (α-HgS) near absolute zero (SI). Such a structural transition is consistent with the relative thermodynamic stability of the two phases: metacinnabar is the stable phase at higher temperature.[22] The transition is also consistent with a reduction in crystallographic symmetry from cubic (β-HgS) to trigonal (α-HgS) as temperature is lowered. A similar transition was reported recently for magnetite which changed structure from cubic to monoclinic at about 125 K.[23] The spectrum of the structurally transformed metacinnabar does not match that of F1-03 at He-T (SI).

We used the bond distances derived for F1-03 at He-T as initial conditions for modeling the RT F1-03 spectrum. A good fit was obtained with two S atoms at 2.35 Å, 0.6 S at 2.57 Å, and 1.6 Hg at 4.14 Å (SI); the 3.25 Å distance was not detected. Like for cinnabar, fewer longer Hg—S and Hg—Hg distances were revealed at RT than at He-T, but none changed significantly (SI). In addition, F1-03 does not match either metacinnabar, which has all Hg—S bonds at 2.51 Å, or cinnabar at RT (SI). Freezing did not change the unique binding between Hg and S in the peat: the multinuclear Hg-SR structure, which is nanosized and surrounded by a relatively flexible organic matrix, is stable.

Organic materials are commonly examined in the frozen state by EXAFS spectroscopy to avoid formation of free radicals that cause photoreduction.[24,25] However, there is virtually no evidence for degraded RT structures during synchrotron measurements of Hg binding to OM,[16−18] likely in part because of the strong bonds that form between Hg and S_{red}. In fact, the small oscillation near 7.8 Å^{-1} at He-T in F1-007 and F1-03 (S_{red}/Hg = 1140 and 220) caused by Hg—Hg pairs is also perceptible in RT spectra of soil OM at S_{red}/Hg = 100 and 20.[18] This is not only further evidence against photoreduction of strongly bound Hg at RT but also supports the conclusion that freezing did not induce the multinuclear structure.

The features of Hg—Hg pairs observed in the He-T spectra of the peats may be visible in the spectra of soil OM at RT[18] because the experimental soil OM—Hg solutions equilibrated for 1 wk[18] compared to 15 h in the peat OM-Hg solutions. Mercury atoms could have had time to move to higher affinity protein-like S_{red} sites even though the soil OM had 75% less S_{red} than the Everglades peats. A similar kinetic effect may have contributed to visualizing the longer bond distances in our He-T analyses given the nine-month interval between the measurements at the two temperatures. In addition, the greater amount of S_{red} in the peats may have accelerated the change in binding enough to detect the multinuclear cluster in the modeled RT spectra despite the short equilibration time. The final pH of our peat experiments was 5−6 vs a pH near 4 for the soil OM.[18] If apparent pK_a values of thiols in peats are in the range of those for plant
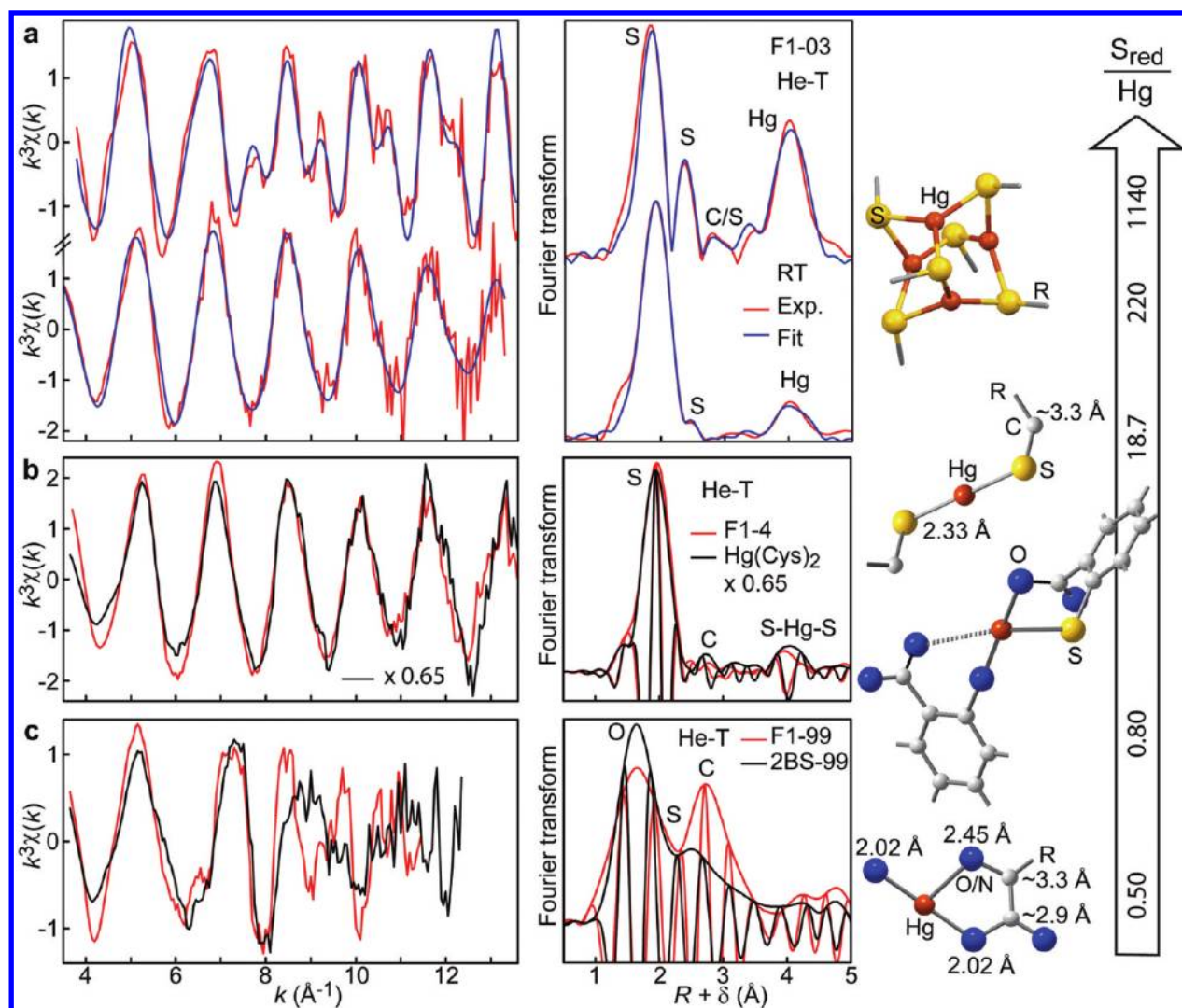
Figure 4. EXAFS spectra, Fourier transforms, and model structures of dominant Hg binding structures (left to right) and correspondence with S_{red}/Hg in the peats (far right). (a) F1−03 (353 ppm Hg) at RT and He-T with model fits. Schematic multinuclear Hg_4S_x structure is at right. Data analysis shows that the Hg—S distance at 2.53−2.57 Å contributes to the right tail of the first peak (SI). Imaginary parts of the Fourier transforms were omitted for clarity. (b) F1-4 (~4100 ppm Hg) and $Hg(Cys)_2$ reference solution at He-T. The modeled $Hg(SR)_2$ structure is shown at the upper right. (c) F1-99 (99100 ppm) and 2BS-99 (99100 ppm) at He-T. A schematic of the five-membered (O,N) chelate ring structure in 2BS-99 is shown at the lower right. Modeled bond distances and coordination numbers in F1-99 suggest the hypothetical structure linking Hg to aromatic rings at the upper right. Atoms coded as oxygen are indistinguishable from nitrogen.

metallothioneins,[26] then accelerated binding of Hg in the peat also could be explained by more deprotonated sites at higher pH.

Similarity of Multinuclear Hg−S Structure to Metal− Thiolate Clusters in Metallothionein Proteins. The average Hg—S structure can be described as a tetrameric cluster (Hg_4S_x) in which three-coordinate molecular units of one Hg atom with two short bonds (2.34 Å) and one longer bond (2.53 Å) to S atoms are arranged so that any two Hg atoms are about 4.12 Å apart (Figure 4a). The bonds around any Hg atom form a Y-shape,[19] precluding successful modeling of the peak at $R + \delta \approx 4$ Å in the Fourier transforms at both temperatures as multiple-scattering from a linear $Hg(SR)_2$ complex[18] (SI). At least 0.5 mol % of S_{red} must be in the cluster, similar to the 0.15−1% deduced for strong binding constants of Hg in other OM samples.[8,9,15]

The Hg_4S_x model cluster resembles polynuclear-thiolate clusters in Cu(I) metalloproteins and metal-peptide compounds.[27]

$Cu(I)_4S_6$-type structures with three-coordinate metal centers occur in metallochaperone and metallothionein (MT) proteins with CXC (CysXaaCys) amino acid consensus sequences from mammals and yeast.[28−32] These structures mimic organometallic $[Cu_4(SPh)_6]^{2-}$, which contains thiolated aromatics.[33]

Structures of Hg metalloproteins are few and varied. One three-coordinate unit with Hg—S bond length of 2.43(2) Å was observed in the merR-regulatory protein,[34] and one with either two 2.34 Å and one 2.47 Å or three 2.39 Å Hg—S bonds in a de novo Hg(II)-metalloprotein.[35] In Hg_7-MT, Hg is bonded to either two S atoms at 2.33(2) Å (and possibly two other S at 3.4 Å)[36] or to three S at 2.42(2) Å,[37] whereas in Hg_{18}-MT Hg is bonded to two S atoms at 2.42(3) Å and one Cl at 2.57 Å;[36] no Hg—Hg distances were reported for either Hg-MT. The crystal structure of the metallochaperone Hah1 in the presence of Hg has a distorted tetrahedral coordination with one Hg bonded to

one S at 2.3 Å, two S at 2.5 Å, and one S at 2.8 Å.[38] One Hg atom is thought to bind to two Hah1 molecules each with CXXC sequences. Molecules with CXXC sequences usually form two-coordinate structures as in the MerP Hg(II) transport protein.[39] Three-coordinate binding in a multinuclear cluster was inferred for Hg-loaded MT from *Cicer arietinum* (chickpea) using UV-vis spectroscopy.[40]

$Hg(SR)_2$, Chelate Ring, and Thiolated Aromatic Structures at Higher Hg Concentrations. A linear $Hg(SR)_2$ structure was dominant in the F1-4 peat with 4180 ppm Hg ($S_{red}/Hg = 18.7$). This structure has the same shorter Hg—S bonds (2.33 Å at He-T and 2.35 Å at RT) as the cluster, but not the longer Hg—S bond (2.53 Å) and Hg—Hg distance (4.12 Å): there is neither a spectral shift to lower k nor extra oscillations at higher k (Figure 4b). The spectrum and Fourier transform at He-T match those for our 1:2 Hg-cysteine solution ($Hg(Cys)_2$), and similarly frozen Hg-cysteine solids,[41] and Hg-cysteine and Hg-glutathione solutions.[41,42] Linearity is confirmed by the peak at $R + \delta \approx 4$ Å in the Fourier transform at He-T, caused by multiple scattering paths (SI). Only 65% of the $Hg(Cys)_2$ spectrum is needed to match the F1—4 spectrum indicating that at least 20—25% of the Hg is bonded to O and/or N (Figure 4b).

The other sample having a dominant binding environment was 2BS-99 (99100 ppm Hg and $S_{red}/Hg = 0.50$). The spectra indicate shorter bonds between Hg and lower Z atoms (Figures 2 and 4c). In the best model, Hg bonds to one O atom at 2.02 Å, one O or N atom at 2.45 Å, one C atom at 2.87 Å, and one C atom at 3.28 Å (SI). The structure is likely a five-membered chelate ring with one carboxylate O and amino N (α-HN_2) or alcohol O (α-OH) from an α-substituted carbon, similar to structures for monomethylmercury binding to amino acids[43,44] and for Hg and Cu(II) complexed to soil OM and humic acid.[18,24]

The second new Hg—S structure appeared in F1-99 (also having 99100 ppm Hg, but a higher S_{red}/Hg of 0.80 compared to 2BS-99). A small oscillation at about 6.7 Å^{-1} and the shift of the third oscillation at 8 Å^{-1} in the He-T spectrum are distinctive (Figure 4c). The best model gives an average structure around Hg of one O or N atom at 2.02 Å, 0.4 S atoms at 2.34 Å, two C atoms at 2.97 Å, and four C atoms at 3.28 Å (SI). The number of C atoms along with S suggests the presence of thiolated aromatic units.[45] However, the low amount of S indicates that this structure is mixed mainly with the (O,N) chelate ring seen in 2BS-99.

The spectra of F1-18 (18400 ppm Hg; $S_{red}/Hg = 4.3$) could not be modeled successfully from first principles because there was no dominant binding environment. Instead, RT and He-T spectra were analyzed by linear combination fitting using spectra from the other peat samples. Sample F1-18 has about 67% F1-4 type bonds and 33% of the mixture of bonds modeled in F1-99 (SI), further supporting a continuum in binding environments.

Environmental Implications. As the concentration of adsorbed Hg increased, the Hg atoms filled increasing amounts of progressively weaker binding sites. Binding of highest to lowest affinity corresponds in order to the Hg_4S_x cluster, linear $Hg(SR)_2$, thiolated aromatic, and five-membered chelate ring sites (Figure 4). The first three reinforce the importance of thiolate ligands even at relatively low values of S_{red}/Hg, where OH and N ligands are in great excess. Other relatively weak binding sites with O and N ligands may exist at low values of S_{red}/Hg, but could not be distinguished in this study. Also, the EXAFS spectroscopic data obtained here cannot be used to differentiate O from N ligands such as the imidazole component of histidine which can bind metals in protein structures.[46] A four-coordinate

Hg-SR structure like that observed, for example, in the HgHah1 metallochaperone protein[38] or the $Hg(Cys)_4$ species in Hg-cysteine solutions with $H_2Cys/Hg(II) > 5$[41] might form at higher values of S_{red}/Hg than investigated here. However, the longer bond-length expected for such a structure[19] was never dominant in the peat samples.

Thiols may be incorporated into OM as components of biomolecules such as metallothioneins and phytochelatins. Metallothioneins, which have high contents of cysteinyl thiols, are produced by bacteria and eukaryoa and possibly by archaea.[26,47,48] Photosynthetic organisms also produce phytochelatins, which are glutathione-based peptides with $(\gamma\text{-Glu-Cys})_n$Gly (PC$_n$, $n = 2-11$). In addition, thiols can be formed when hydrogen sulfide, typically generated by bacterial sulfate reduction,[49-51] adds to unsubstituted double bonds in alkenes and aromatics from tannins, lignins, and terpenoids.[52,53]

Reduced sulfur in the peats has XANES character like that of thiols in cysteine and disulfide bridges in cystine (SI); that is, the reduced sulfur that forms metal—thiolate clusters in metalloproteins. Such clusters typically have 2—11 metal centers[54] with evidence in bacterial, animal, and plant MTs that histidine residues stabilize the negative charge of the cluster.[55] Histidine residues can also be part of the coordination structure.[46] Values equal to 2—2.7 observed for the ratios of protons exchanged for low amounts of adsorbed Hg in DOM and soil OM at pH ≤ 7[10,13] imply $x = 8-11$ in the Hg_4S_x structure, in the range of typical numbers of S atoms in MT metal—thiolate clusters.

Living organisms can control the binding of metals to stable clusters in MTs by cellular redox reactions[56,57] and rapid metal exchange can occur through protein folding and unfolding.[58] Metal—thiolate clusters in plant MTs tend to be somewhat less stable than those in most vertebrate MTs at comparable pH,[26,59] which may be related to fewer cysteine residues and longer linker chains between domains in plant MTs. Upon cellular death, metal—thiolate clusters might become incorporated in OM whereas amino acid linker segments likely decompose.

Mercury(II) binds more strongly than Cu(I), Cd(II), Pb(II), and Zn(II) to MTs and model peptides in vitro[60-62] and in phytochelatins the strength of metal binding is higher with length of the peptides (i.e., with more cysteine).[63,64] Phytochelatin—metal complexes can be stabilized if plants or fungi produce excess sulfide.[65-67] Phytochelatins, MTs, and intracellular sulfide production may all explain Hg-rich granules in roots of plants grown in vivo[68-70] and in a contaminated saltmarsh.[71]

In the Everglades peats, the S_{red} in the thiolate ligands that formed the experimental Hg_4S_x type of clusters may originate as cysteine in MTs or phytochelatins in sawgrass (2BS), cattail (F1) (SI), and periphyton[72] or in MTs produced by aquatic invertebrates,[73] fungi, and bacteria. Thiols also could have been added to the peats during bacterial reduction of aqueous sulfate.[20]

The two new Hg-SR structures we identified may elucidate other interactions between OM and Hg species. Formation of mercury-thiolate clusters might explain why metacinnabar was inhibited from precipitating in DOM solutions to which Hg was added first ($<5 \times 10^{-8}$ M; $S_{red}/Hg \sim 60$) followed by sulfide.[74] A thiolated aromatic structure could clarify why cinnabar dissolution rates increased with greater aromaticity of DOM and not reduced sulfur content.[75,76] Multinuclear clusters might be retained and/or nucleate HgS minerals as peat transforms to coal during burial. This is supported by isotopic signatures of presumed organic-bound vs hydrothermally sourced Hg in coal.[77]

Mercury-SR bonds, in general, could also explain the origin of Hg in petroleum or natural gas.

The observed Hg-SR structures raise other questions. What is the origin of the mercury-thiolate cluster? Are metalloproteins and peptides added to peat directly from plants and other organisms living in the aquatic environment? If so, did the Hg added during the experiments displace other trace metals originally complexed in these biomolecules? Is the Hg_4S_x cluster the strongest binding site for Hg in peat and by implication other forms of natural organic matter, and if so, is this Hg available or unavailable for methylation? Further characterization of specific biomolecules in macromolecular natural organic matter would be a step forward toward linking cellular functions in living organisms to sequestration of trace metals by organic materials in the earth.

■ ASSOCIATED CONTENT

ⓈSupporting Information. Descriptions of methods. Adsorption isotherms. Model fits of S-K edge XANES and Hg-L$_3$ EXAFS spectra with tables of fit parameters. Microfluorescence and microdiffraction analysis for S and Fe—S species. This material is available free of charge via the Internet at http://pubs.acs.org.

■ AUTHOR INFORMATION

Corresponding Author
*Phone: (312) 355-3276; e-mail: klnagy@uic.edu.

Present Addresses
[⊥]Integral Consulting Inc., 285 Century Place, Suite 190, Louisville, Colorado 80027.

■ ACKNOWLEDGMENT

■ REFERENCES

(1) Benoit, J. M.; Gilmour, C. C.; Mason, R. P.; Heyes, A. Sulfide controls on mercury speciation and bioavailability to methylating bacteria in sediment pore waters. *Environ. Sci. Technol.* **1999**, *33*, 951–957.

(2) Schaefer, J. K.; Morel, F. M. M. High methylation rates of mercury bound to cysteine by *Geobacter sulfurreducens*. *Nat. Geosci.* **2009**, *2*, 92–93.

(3) Pickhardt, P. C.; Fisher, N. S. Accumulation of inorganic and methylmercury by freshwater phytoplankton in two contrasting water bodies. *Environ. Sci. Technol.* **2007**, *41*, 125–131.

(4) Gorski, P. R.; Armstrong, D. E.; Hurley, J. P.; Krabbenhoft D. P. Influence of natural dissolved organic carbon on the bioavailability of mercury to a freshwater alga. *Environ. Pollut.* **2008**, *154* 116–123.

(5) Hammerschmidt, C. R.; Fitzgerald, W. F.; Balcom, P. H.; Visscher, P. T. Organic matter and sulfide inhibit methylmercury production in sediments of New York/New Jersey Harbor. *Mar. Chem.* **2008**, *109*, 165–182.

(6) Cheesman, B. V.; Arnold, A. P.; Rabenstein, D. L. Nuclear magnetic resonance studies of the solution chemistry of metal complexes. 25. Hg(thiol)3 complexes and Hg(II)-thiol ligand exchange kinetics. *J. Am. Chem. Soc.* **1988**, *110*, 6359–6364.

(7) Skyllberg, U.; Xia, K.; Bloom, P. R.; Nater, E. A.; Bleam, W. F. Binding of mercury to reduced sulfur in soil organic matter along upland-peat soil transects. *J. Environ. Qual.* **2000**, *29*, 855–865.

(8) Haitzer, M.; Aiken, G. R.; Ryan, J. N. Binding of mercury(II) to dissolved organic matter: The role of the mercury-to-DOM concentration ratio. *Environ. Sci. Technol.* **2002**, *36*, 3564–3570.

(9) Drexel, R. T.; Haitzer, M.; Ryan, J. N.; Aiken, G. R.; Nagy, K. L. Mercury(II) sorption to two Florida Everglades peats: Evidence for strong and weak binding and competition by dissolved organic matter released from the peat. *Environ. Sci. Technol.* **2002**, *36*, 4058–4064.

(10) Haitzer, M.; Aiken, G. R.; Ryan, J. N. Binding of mercury(II) to aquatic humic substances: Influence of pH and source of humic substances. *Environ. Sci. Technol.* **2003**, *37*, 2436.

(11) Hsu-Kim, H.; Sedlak, D. L. Strong Hg(II) complexation in municipal wastewater effluent and surface waters. *Environ. Sci. Technol.* **2003**, *37*, 2743–2749.

(12) Han, S.; Gill, G. A. Determination of mercury complexation in coastal and estuarine waters using competitive ligand exchange method. *Environ. Sci. Technol.* **2005**, *39*, 6607–6615.

(13) Khwaja, A. R.; Bloom, P. R.; Brezonik, P. L. Binding constants of divalent mercury (Hg^{2+}) in soil humic acids and soil organic matter. *Environ. Sci. Technol.* **2006**, *40*, 844–849.

(14) Gasper, J. D.; Aiken, G. R.; Ryan, J. N. A critical review of three methods used for the measurement of mercury (Hg^{2+})-dissolved organic matter stability constants. *Appl. Geochem.* **2007**, *22*, 1583–1597.

(15) Skyllberg, U. Competition among thiols and inorganic sulfides and polysulfides for Hg and MeHg in wetland soils and sediments under suboxic conditions: Illumination of controversies and implications for MeHg net production. *J. Geophys. Res.* **2008**, *113*, 1–14.

(16) Xia, K.; Skyllberg, U. L.; Bleam, W. F.; Bloom, P. R.; Nater, E. A.; Helmke, P. A. X-ray absorption spectroscopic evidence for the complexation of Hg(II) by reduced sulfur in soil humic substances. *Environ. Sci. Technol.* **1999**, *33*, 257–261.

(17) Hesterberg, D.; Chou, J. W.; Hutchison, K. J.; Sayers, D. E. Bonding of Hg(II) to reduced organic sulfur in humic acid as affected by S/Hg ratio. *Environ. Sci. Technol.* **2001**, *35*, 2741–2745.

(18) Skyllberg, U.; Bloom, P. R.; Qian, J.; Lin, C.-M.; Bleam, W. F. Complexation of mercury(II) in soil organic matter: EXAFS evidence for linear two-coordination with reduced sulfur groups. *Environ. Sci. Technol.* **2006**, *40*, 4174–4180.

(19) Manceau, A.; Nagy, K. L. Relationships between Hg(II)-S bond distance and Hg(II) coordination in thiolates. *Dalton Trans.* **2008**, 1421–1425.

(20) Gilmour, C. C.; Riedel, G. S.; Ederington, M. C.; Bell, J. T.; Gill, G. A.; Stordal, M. A. Methylmercury concentrations and production rates across a trophic gradient in the northern Everglades. *Biogeochemistry* **1998**, *40*, 327–345.

(21) Jew, A. D.; Kim, C. S.; Rytuba, J. J.; Gustin, M. S.; Brown, G. E., Jr. New technique for quantification of elemental Hg in mine wastes and its implications for mercury evasion into the atmosphere. *Environ. Sci. Technol.* **2011**, *45*, 412–417.

(22) Potter, R. W.; Barnes, H. L. Phase relations in the binary Hg-S. *Am. Mineral.* **1978**, *63*, 1143–1152.

(23) Kasama, T.; Church, N. S.; Feinberg, J. M.; Dunin-Borkowski, R. E.; Harrison, R. J. Direct observation of ferrimagnetic/ferroelastic

domain interactions in magnetite below the Verwey transition. *Earth Planet. Sci. Lett.* **2010**, *297*, 10–17.

(24) Manceau, A.; Matynia, A. The nature of Cu bonding to natural organic matter. *Geochim. Cosmochim. Acta* **2010**, *74*, 2556–2580.

(25) Andrews, J. C. Mercury speciation in the environment using X-ray absorption spectroscopy. *Struct. Bonding (Berlin, Ger.)* **2006**, *120*, 1–35.

(26) Freisinger, E. Plant MTs-long neglected members of the metallothionein superfamily. *Dalton Trans.* **2008**, *47*, 6649–6852.

(27) Pickering, I. J.; George, G. N.; Dameron, C. T.; Kurz, B.; Winge, D. R.; Dance, I. G. X-ray absorption spectroscopy of cuprous-thiolate clusters in proteins and model systems. *J. Am. Chem. Soc.* **1993**, *115*, 9498–9505.

(28) Brown, K. R.; Keller, G. L.; Pickering, I. J.; Harris, H. H.; George, G. N.; Winge, D. R. Structures of the cuprous-thiolate clusters of the Mac1 and Ace1 transcriptional activators. *Biochemistry* **2002**, *41*, 6469–6476.

(29) Xiao, Z.; Loughlin, F.; George, G. N.; Howlett, G. J.; Wedd, A. G. C-terminal domain of the membrane copper transporter Ctr1 from *Saccharomyces cerevisiae* binds four Cu(I) ions as a cuprous-thiolate polynuclear cluster: Sub-femtomolar Cu(I) affinity of three proteins involved in copper trafficking. *J. Am. Chem. Soc.* **2004**, *126*, 3081–3090.

(30) Voronova, A.; W., M.-K.; Meyer, T.; Rompel, A.; Krebs, B.; J., K.; Sillard, R.; Palumaa, P. Oxidative switches in functioning of mammalian copper chaperone Cox17. *Biochem. J.* **2007**, *408*, 139–148.

(31) Stasser, J. P.; Siluvai, G. S.; Barry, A. N.; Blackburn, N. J. A multinuclear copper(I) cluster forms the dimerization interface in copper-loaded human copper chaperone for superoxide dismutase. *Biochemistry* **2007**, *46*, 11845–11856.

(32) Bogumil, R.; Faller, P.; P.-A., B.; Vašák, M.; Charnock, J. M.; Garner, C. D. Structural characterization of Cu(I) and Zn(II) sites in neuronal-growth-inhibitory factor by extended X-ray absorption fine structure (EXAFS). *Eur. J. Biochem.* **1998**, *255*, 172–177.

(33) Dance, I. G.; Calabrese, J. C. The crystal and molecular structure of the hexa-($\mu_2$benzenethiolato)tetracuprate(I) dianion. *Inorg. Chim. Acta* **1976**, *19*, L41–L42.

(34) Wright, J. G.; Tsang, H.-T.; Penner-Hahn, J. E.; O'Halloran, T. V. Coordination chemistry of the Hg-MerR metalloregulatory protein: Evidence for a novel tridentate Hg-cysteine receptor site. *J. Am. Chem. Soc.* **1990**, *112*, 2434–2435.

(35) Dieckmann, G. R.; McRorie, D. K.; Tierney, D. L.; Utschig, L. M.; Singer, C. P.; O'Halloran, T. V.; Penner-Hahn, J. E.; DeGrado, W. F.; Pecoraro, V. L. *De novo* design of mercury-binding two- and three-helical bundles. *J. Am. Chem. Soc.* **1997**, *119*, 6195–6196.

(36) Jiang, D. T.; Heald, S. M.; Sham, T. K.; Stillman, M. J. Structures of the cadmium, mercury, and zinc thiolate clusters in metallothionein: XAFS study of Zn7-MT, Cd7-MT, Hg7-MT, and Hg18-MT formed from rabbit liver metallothionein 2. *J. Am. Chem. Soc.* **1994**, *116*, 11004–11013.

(37) Hasnain, S. S. Application of EXAFS to biochemical systems. *Top. Curr. Chem.* **1988**, *147*, 73–93.

(38) Wernimont, A. K.; Huffman, D. L.; Lamb, A. L.; O'Halloran, T. V.; Rosenzwieg, A. C. Structural basis for copper transfer by the metallochaperone for the Menkes/Wilson disease proteins. *Nat. Struct. Biol.* **2000**, *7*, 766–771.

(39) Steele, R. A.; Opella, S. J. Structures of the reduced and mercury-bound forms of MerP, the periplasmic protein from the bacterial mercury detoxification system. *Biochemistry* **1997**, *36*, 6885–6895.

(40) Schict, O.; Freisinger, E. Spectroscopic characterization of *Cicer arietinum* metallothionein 1. *Inorg. Chim. Acta* **2009**, *362*, 714–724.

(41) Jalilehvand, F.; Leung, B. O.; Izadifard, M.; Damian, E. Mercury-(II) cysteine complexes in alkaline aqueous solution. *Inorg. Chem.* **2006**, *45*, 66–73.

(42) Mah, V.; Jalilehvand, F. Mercury(II) complex formation with glutathione in alkaline aqueous solution. *J. Biol. Inorg. Chem.* **2008**, *13*, 541–553.

(43) Alex, S.; Savoie, R.; Corbeil, M.-C.; Beauchamp, A. L. Complexation of glycylglycine by the methylmercury cation: a vibrational spectroscopy and X-ray diffraction study. *Can. J. Chem.* **1986**, *64*, 148–157.

(44) Corbeil, M.-C.; Beauchamp, A. L.; Alex, S.; Savoie, R. Interaction of the methylmercury cation with glycine and alanine: a vibrational and X-ray diffration study. *Can. J. Chem.* **1986**, *64*, 1876–1884.

(45) Alvarez-Puebla, R. A.; Valenzuela-Calahorro, C.; Garrido, J. J. Theoretical study on fulvic acid structure, conformation and aggregation: a molecular modeling approach. *Sci. Total Environ.* **2006**, *358*, 243–254.

(46) Penner-Hahn, J. E. Characterization of "spectroscopically quiet" metals in biology. *Coord. Chem. Rev.* **2005**, *249*, 161–177.

(47) Waldron, K. J.; Robinson, N. J. How do bacterial cells ensure that metalloproteins get the correct metal? *Nat. Rev. Microbiol.* **2009**, *6*, 25–35.

(48) Morris, C. A.; Nicolaus, B.; Sampson, V.; Harwood, J. L.; Kille, P. Identification and characterization of a recombinant metallothionein protein from a marine alga, *Fucus vesiculosus. Biochem. J.* **1999**, *338*, 553–560.

(49) Casagrande, D. J.; Gronli, K.; Sutton, N. The distribution of sulfur and organic matter in various fractions of peat: origins of sulfur in coal. *Geochim. Cosmochim. Acta* **1980**, *44*, 25–32.

(50) Francois, R. A study of sulphur enrichment in the humic fraction of marine sediments during early diagenesis. *Geochim. Cosmochim. Acta* **1987**, *51*, 17–27.

(51) Ferdelman, T. G.; Church, T. M.; Luther, G. W., III Sulfur enrichment of humic substances in a Delaware salt marsh sediment core. *Geochim. Cosmochim. Acta* **1991**, *55*, 979–988.

(52) Herkorn, N.; Benner, R.; Frommberger, M.; Schmitt-Kopplin, P.; Witt, M.; Kaiser, K.; Kettrup, A.; Hedges, J. I. Characterization of a major refractory component of marine dissolved organic matter. *Geochim. Cosmochim. Acta* **2006**, *70*.

(53) Lam, B.; Baer, A.; Alaee, M.; Lefebvre, B.; Moser, A.; Williams, A.; Simpson, A. J. Major structural components in freshwater dissolved organic matter. *Environ. Sci. Technol.* **2007**, *41*, 8240–8247.

(54) Presta, A.; Fowle, D. A.; Stillman, M. J. Structural model of rabbit liver copper metallothionein. *Dalton Trans.* **1997**, 977–984.

(55) Blindauer, C. A.; Razi, M. T.; Campopiano, D. J.; Sadler, P. J. Histidine ligands in bacterial metallothionein enhance cluster stability. *J. Biol. Inorg. Chem.* **2007**, *12*, 393–405.

(56) Maret, W.; Vallee, B. L. Thiolate ligands in metallothionein confer redox activity on zinc clusters. *Proc. Natl. Acad. Sci. U. S. A.* **1998**, *95*, 3478–3482.

(57) Song, F.; Briseno, A. L.; Zhou, F. Redox reactions of and transformation between cysteine-mercury thiolate and cystine in metallothioneins adsorbed at a thin mercury film electrode. *Langmuir* **2001**, *17*, 4081–4089.

(58) Duncan, K. E. R.; Ngu, T. T.; Chan, J.; Salgado, M. T.; Merrifield, M. E.; Stillman, M. J. Peptide folding, metal-binding mechanisms, and binding site structures in metallothioneins. *Exp. Biol. Med.* **2006**, *231*, 1488–1499.

(59) Robinson, N. J.; Tommey, A. M.; Kuske, C.; Jackson, P. J. Plant metallothioneins. *Biochem. J.* **1993**, *295*, 1–10.

(60) Vašák, M., Metal removal and substitution in vertebrate and invertebrate metallothioneins. *Methods Enzymol.* Eds.; **1991**, *205*, 452–458.

(61) Stillman, M. J. Metallothioneins. *Coord. Chem. Rev.* **1995**, *144* 461–511.

(62) Rousselot-Pailley, P.; Sénèque, O.; Lebrun, C.; Crouzy, S.; Boturyn, D.; Dumy, P.; Ferrand, M.; P., D. Model peptides based on the binding loop of the copper metallochaperone Atx1: Selectivity of the consensus sequence MxCxxC for metal ions Hg(II), Cu(I), Pb(II), and Zn(II). *Inorg. Chem.* **2006**, *45*, 5510–5520.

(63) Mehra, R. K.; Miclat, J.; Kodati, V. R.; Abdullah, R.; Hunter, T. C.; Mulchandani, P. Optical spectroscopic and reverse-phase HPLC analyses of Hg(II) binding to phytochelatins. *Biochem. J.* **1996**, *314*, 73–82.

(64) Checkmeneva, E.; Diaz-Cruz, J. M.; Arino, C.; Esteban, M. Binding of Hg^{2+} with phytochelatins: Study by differential pulse voltammetry on rotating Au-disk electrode, electrospray ionization mass-spectrometry, and isothermal titration calorimetry. *Environ. Sci. Technol.* **2009**, *43*, 7010–7015.

(65) Reese, R. N.; Winge, D. R. Sulfide stabilization of the cadmium-γ-glutamyl peptide complex of *Schizosaccharomyces pombe. J. Biol. Chem.* **1988**, *263*, 12832–12835.

(66) Steffens, J. C. The heavy-metal binding peptides of plants. *Annu. Rev. Plant Physiol. Plant Mol. Biol.* **1990**, *41*, 553–575.

(67) Dameron, C. T.; Reese, R. N.; Mehra, R. K.; Kortan, A. R.; Carroll, P. J.; Steigerwald, M. L.; Brus, L. E.; Winge, D. R. Biosynthesis of cadmium sulphide quantum semiconductor crystallites. *Nature* **1989**, *338*, 596–597.

(68) Velasco-Alinsug, M. P.; Rivero, G. C.; Quibuyen, T. A. O. Isolation of mercury-binding peptides in vegetative parts of *Chromolaena odorata*. *Z. Naturforsch., C: J. Biosci.* **2005**, *60c*, 252–259.

(69) Iglesia-Turiño, S.; Febrero, A.; Jauregui, O.; Caldelas, C.; Araus, J. L.; J., B. Detection and quantification of unbound phytochelatin 2 in plant extracts of *Brassica napus* growth with different levels of mercury. *Plant Physiol.* **2006**, *142*, 742–749.

(70) Patty, C.; Barnett, B.; Mooney, B.; Kahn, A.; Levy, S.; Liu, Y.; Pianetta, P.; Andrews, J. C. Using X-ray microscopy and Hg L3 XANES to study Hg binding in the rhizosphere of *Spartina* cordgrass. *Environ. Sci. Technol.* **2009**, *43*, 7397–7402.

(71) Válega, M.; Lima, A. I. G.; Figueira, E. M. A. P.; Pereira, E.; Pardal, M. A.; Duarte, A. C. Mercury intracellular partitioning and chelation in a salt marsh plant, *Halimione portulacoides* (L.) Aellen: Strategies underlying tolerance in environmental exposure. *Chemosphere* **2009**, *74*.

(72) Perales-Vela, H. G.; Peña-Castro, J. M.; Cañizares-Villanueva, R. O. Heavy metal detoxifiation in eukaryotic microalgae. *Chemosphere* **2006**, *64*, 1–10.

(73) Amiard, J.-C.; Amiard-Triquet, C.; Barka, S.; Pellerin, J.; Rainbow, P. S. Metallothioneins in aquatic invertebrates: Their role in metal detoxification and their use as biomarkers. *Aquat. Toxicol.* **2006**, *76*, 160–202.

(74) Ravichandran, M.; Aiken, G. R.; Ryan, J. N.; Reddy, M. M. Inhibition of precipitation and aggregation of metacinnabar (mercuric sulfide) by dissolved organic matter isolated from the Florida Everglades. *Environ. Sci. Technol.* **1999**, *33*, 1418–1423.

(75) Ravichandran, M.; Aiken, G. R.; Reddy, M. M.; Ryan, J. N. Enhanced dissolution of cinnabar (mercuric sulfide) by dissolved organic matter isolated from the Florida Everglades. *Environ. Sci. Technol.* **1998**, *32*, 3305–3311.

(76) Waples, J. S.; Nagy, K. L.; Aiken, G. R.; Ryan, J. N. Dissolution of cinnabar (HgS) in the presence of natural organic matter. *Geochim. Cosmochim. Acta* **2005**, *69*, 1575–1588.

(77) Lefticariu, L.; Blum, J. D.; Gleason, J. D. Mercury isotope evidence for multiple mercury sources in coal from the Illinois Basin. *Environ. Sci. Technol.* **2011**, *45*, 1724–1729.